A CELESTIAL REFERENCE FRAME AT X/KA-BAND (8.4/32 GHZ) FOR DEEP SPACE NAVIGATION

C. S. Jacobs[1], J.E. Clark[2], C. García-Miró[3], S. Horiuchi[4], A. Romero-Wolf[5], L. Snedeker[6], and I. Sotuela[7]

[1]*Jet Propulsion Laboratory, California Institute of Technology, 4800 Oak Grove Dr., Pasadena CA 91109, 818-354-7490, Christopher.S.Jacobs@jpl.nasa.gov*

[2]*Jet Propulsion Laboratory, California Institute of Technology, 4800 Oak Grove Dr., Pasadena CA 91109, (818)393-5994, John.E.Clark@jpl.nasa.gov*

[3]*INTA/NASA, Madrid Deep Space Com. Complex, Paseo del Pintor Rosales, 34 bajo, E-28008, Spain, 34-91-867-7130, cgmiro@mdscc.nasa.gov*

[4]*CSIRO/NASA, Canberra Deep Space Com. Complex, PO Box 1035, AU Tuggeranong ACT 2901, Australia, phone, shoriuchi@cdscc.nasa.gov*

[5]*Jet Propulsion Laboratory, California Institute of Technology, 4800 Oak Grove Dr., Pasadena CA 91109, 818-354-0058, Andrew.Romero-Wolf@jpl.nasa.gov*

[6]*ITT Exelis, 1400 Shamrock Avenue Monrovia, CA 91016, (760)255-8259, lgsnedeker@gdscc.nasa.gov*

[7]*INTA/NASA, Madrid Deep Space Com. Complex, Paseo del Pintor Rosales, 34 bajo, E-28008, Spain, 34-91-867-7053, isotuela@mdscc.nasa.gov*

Abstract: *Deep space tracking and navigation are done in a quasi-inertial reference frame based upon the angular positions of distant active galactic nuclei (AGN). These objects, which are found at extreme distances characterized by median redshifts of z = 1, are ideal for reference frame definition because they exhibit no measurable parallax or proper motion. They are thought to be powered by super massive black holes whose gravitational energy drives galactic sized relativistic jets. These jets produce synchrotron emissions which are detectable by modern radio techniques such as Very Long baseline Interferometry (VLBI).*

We have constructed a reference frame based on sixty-seven X/Ka-band (8.4/32 GHz) VLBI observing sessions (2005 to present), each of ∼24 hours duration, using the intercontinental baselines of NASA's Deep Space Network (DSN): Goldstone, California to Madrid, Spain and Canberra, Australia. We detected 482 sources covering the full 24 hours of Right ascension and declinations down to -45°. Comparison of 460 X/Ka sources in common with the international standard ICRF2 at S/X-band (2.3/8.4 GHz) shows wRMS agreement of 180 μas in $\alpha\cos\delta$ and 270 μas in δ. There is evidence for systematic errors at the 100 μas level. Known errors include limited SNR, lack of phase calibration, troposphere mismodelling, and limited southern geometry. Compared to S/X-band frames (e.g. ICRF2 (Ma et al, 2009)), X/Ka-band allows access to more compact source morphology and reduced core shift. Both these improvements allow for a more well-defined and stable reference frame at X/Ka-band.

In the next decade, the optically-based Gaia mission (Lindegren, 2008) may produce a frame with competitive precision. By accurately registering radio frames with Gaia, we could study wavelength dependent systematic errors. A simulated frame tie between our X/Ka radio frame and the Gaia optical frame predicts a frame tie precision of 10–15 μas (1-σ, per 3-D rotation component) with anticipated radio improvements reducing that to 5–10 μas by Gaia's end of mission ∼2021.

Keywords: *Reference Frame, VLBI, Active Galactic Nuclei, Ka-band, ICRF*

1. Introduction

This article will discuss a celestial reference frame based on radio interferometric observations of distant extragalactic radio sources which is useful for spacecraft tracking and navigation.

Since ancient times navigators have used celestial objects to guide the course of their craft. At the precisions achievable centuries ago, the positions of even nearby stars (a few 10s of light years) were essentially fixed after accounting for a very slow precession of the Earth's pole. As precision improved, especially after the invention of the telescope, it became necessary to account for several types of stellar motion. In 1718 Edmund Halley discovered proper motion of individual stars [11]. In 1727 James Bradley discovered annual aberration due to the Earth's orbital velocity [4]. In 1748, it was again Bradley who discovered nutation of the Earth's pole principally due to torques from the Sun and moon [5]. And it was 1838 before Bessel convincingly detected the finite distances to nearby stars by measuring annual parallax [2]. Based on the foundation of these discoveries, optical reference frames continued to improve leading to the Fundamental Catalogs of the 20th century such as FK4 and FK5 [7].

As useful as the optical catalogs were, a few factors make them less than ideal for modern spacecraft navigation requiring nano-radian (nrad) level position accuracy. First, the motions of stars in the optical domain are not well modelled at the nano-radian level. Even in the best optical catalog, HIPPARCOS [27], positions at the mid-epoch of the mission are accurate to only several nrad and degrade at the level of $\sim$5 nrad/year due to proper motion uncertainty. Second, optical observations are difficult if not impossible during cloudy conditions and other bad weather.

Radio interferometers overcome both these issues as their resolution with VLBI allows catalogs at the 0.5 nrad level of accuracy and observing is reasonably robust at X-band even during rainy conditions. Celestial reference frames based on radio interferometry are routinely used to navigate spacecraft directly as well as to provide supporting calibrations for navigation such as earth orientation measurements and alignment of planetary ephemerides to the radio frame [8].

Thus motivated by the need to navigate inter-planetary space probes, the NASA Deep Space Network (DSN) constructs VLBI radio reference frames to measure spacecraft positions and motions. An earlier version of the DSN catalog was built at S/X-bands and is still periodically maintained. However, because higher spacecraft telemetry rate requirements are driving the DSN to higher frequencies from X-band (8.4 GHz) to Ka-band (32 GHz), the radio catalog presented here was realized at X/Ka bands. Fortuitously, the jump to Ka-band has the astrophysical advantages of more compact source morphology and reduced frequency dependence of the central core ('core shift') which should eventually allow more accurate position determinations. Spacecraft tracking has already been proven at Ka-band as demonstrated by the tracking of the Mars Reconnaissance Orbiter at Ka-band [32].

We also note that international Ka-band acceptance is growing. About 20 antennas around the world have, will have, or are considering acquiring 32 GHz capability. Jacobs *et al* [15] discuss the

potential for a worldwide Ka-band VLBI network capable of high resolution imaging and astrometry of the most compact regions of Active Galactic Nuclei.

This paper is organized as follows: Section 2 presents the advantages and disadvantages of Ka-band observations. Section 3 describes the Ka-band VLBI observations. Section 4 documents our delay modelling. Section 5 presents the resulting radio catalog. Section 6 examines the known sources of error. Section 7 discusses the potential for improving the geometry of our network by adding a southern station. Section 8 presents the potential for a frame tie to the Gaia optical reference frame.

2. Reference frames realization at higher radio frequencies

The recent move of radio observations towards higher frequencies is beginning to provide very promising astrometric results ([18], [6]). Ka-band (32 GHz), approximately a factor of four higher than the usual X-band (8.4 GHz), has several remarkable advantages. For our work in the DSN, the driver is the increase of telemetry data rates and the usage of smaller and lighter radio frequency systems in the spacecraft.

Advantages: The spatial distribution of the observed source flux density becomes significantly more compact [6] and should therefore lead to more stable positions. By moving away from S/X-band observations, S-band Radio Frequency Interference (RFI) problems are avoided. In addition, the ionosphere and solar plasma effects on group delay and signal coherence are reduced by a factor of $\sim$15 allowing observations closer to the Sun and the Galactic Center when single frequency spacecraft observations are made.

Disadvantages: The increase in frequency also implies several disadvantages. It moves the observer closer to the water vapor line at 22 GHz and thus increases the system temperature to up to 10–15 K per atmospheric thickness or more, thereby greatly decreasing sensitivity during humid or poor weather. Furthermore, the sources themselves are in general weaker and many sources are resolved. Also, the coherence times are shortened so that practical integration times are a few minutes or less. Lastly, the antenna pointing accuracy requirements must be tightened by the same factor of four. The combined effect of these disadvantages is to reduce the system's sensitivity. Fortunately, advances in recent years in recording technology (e.g. [39]) make it feasible and affordable to offset these losses in sensitivity by recording at higher data rates.

Thus while the first few years of X/Ka data presented in this paper used the same overall 112 Mbps bit rate as previous S/X work, the recent data were taken at a 4 times higher rate—with an increase to 8–16 times higher rate hoped for within the next year or two.

3. The VLBI Observations

The results presented here are from sixty seven Very Long Baseline Interferometry (VLBI) observing sessions of $\sim$24 hour duration done from July 2005 until June 2012 using NASA's Deep Space Stations (DSS) 25 or 26 in Goldstone, California to either DSS 34 in Tidbinbilla, Australia or DSS 55 outside Madrid, Spain to form interferometric baselines of 10,500 and 8,400 km length, respectively. We recorded VLBI data simultaneously at X-band (8.4 GHz) and Ka-band (32 GHz).

Initially, sampling of each band was at 56 Mbps while more recent passes used 160/288 Mbps at X/Ka-bands, respectively. Each band used a spanned a bandwidth of $\sim$360 MHz. The data were filtered, sampled, and recorded to the Mark-4 or Mark-5A VLBI systems. The data were then correlated with the JPL BlockII correlator [25] or the JPL SOFTC software correlator [22]. Fringe fitting was done with the FIT fringe fitting software [21]. This procedure resulted in 20,128 pairs of group delay and phase rate measurements covering the full 24 hours of right ascension and declinations down to -45°. Individual observations were $\sim$2 minutes duration in the early, lower data rate sessions. Observations were shortened to $\sim$1 minute in the more recent higher rate sessions.

4. Modelling

The observations described above were then modelled using the MODEST software [33]. The a priori Earth orientation was the MHB nutation model [24] coupled with the empirically determined UT1-UTC and Polar Motion of the Space 2010 series [29]. A linear drift correction for the celestial pole vs. time was estimated on top of the a priori nutation/precession model. The celestial frame was aligned to the ICRF2 defining sources [23] using a No-Net-Rotation constraint [14]. Station velocities were estimated; station locations were estimated with a 1 cm constraint per component to a decades-long S/X-band VLBI solution.

5. Results

The above described observations produced detections of 482 extragalactic radio sources. The data set was analyzed using a multi-parameter least-squares adjustment which estimated the Right Ascensions and Declinations of the 482 sources along with baseline vectors, and session specific instrumental and tropospheric parameters. Fig. 1 shows the distribution of the 482 sources over the celestial sphere using a Hammer-Aitoff projection to preserve the areal surface density of the distribution.

Several characteristics are worth noting. First, the distribution, while covering the northern hemisphere, only does down to -45° declination in the south. This is because we only have one southern station (Australia) and thus we have no all-southern baselines with which to reach the south polar cap. Sec. 7, below, will discuss our plans to remedy this geometrical imbalance.

Second, the ecliptic plane (indicated by the dashed blue-grey line) is of special importance to our application of inter-planetary spacecraft navigation as that plane is where the spacecraft spend most of their time. Accordingly, we are working to densify our frame along the ecliptic. For example, the southern ecliptic from $\alpha = 12h$ to $14h$, $\delta = 0^\circ$ to -15° was densified in preparation for the **Mars Science Laboratory** mission.

Third, the galactic plane (indicated by the dashed yellow-red line) is an area of special challenge. Source finding surveys for extra-galactic sources routinely avoid this region because of the difficulties of separating galactic and extra-galactic sources. Even when attempts are made to observe near the galactic plane, extragalactic signals are scattered by the inter-stellar media (ISM) of the galaxy which causes the source size to broaden (de-focus) in proportion to the wavelength squared.

This quadratic dependence makes it especially difficult to observe near the galactic plane at lower frequencies such as S-band. This issue is of current interest because the **Mars 2016 'InSight'** mission is planning its trajectory along the southern ecliptic very near the galactic center. **InSight** is expected to encounter Mars at about $\alpha = 18h$, $\delta = -26^\circ$. Note the low density of sources in this region and furthermore the low precision of the few sources which are in that area.

Fourth, source position precision generally degrades as one moves southward. In Fig. 1a, we see that at about $\delta = -20^\circ$ the Right Ascension precision suddenly gets worse. This is because -20° is about as far south as our California to Spain baseline can see. Sources below this limit depend on just the single baseline from California to Australia. In Fig. 1b, we see a similar degradation in declination precision going southward. In addition—ignoring the north polar cap—the overall precisions are worse for declinations compared to Right Ascensions. This is because we have only one baseline, California-Australia, which has a significant north-south baseline component with which to measure declinations. The polar caps are a special case because the rotation of the Earth provides perpendicular baselines after 6 hours of rotation thereby giving good measurements of both α and δ from a single rotating baseline.

The issue of precision degradation is of special concern in the southern ecliptic because many of the uncertainties in α and almost all of the uncertainties in δ have not yet met the nominal 1.0 nrad requirement for deep space navigation. While additional observations with the current system will be of some help, we believe that it is essential to improve our network geometry in order to make significant progress toward uniform precision over the entire celestial sphere. This issue is discussed further in Sec. 7 below.

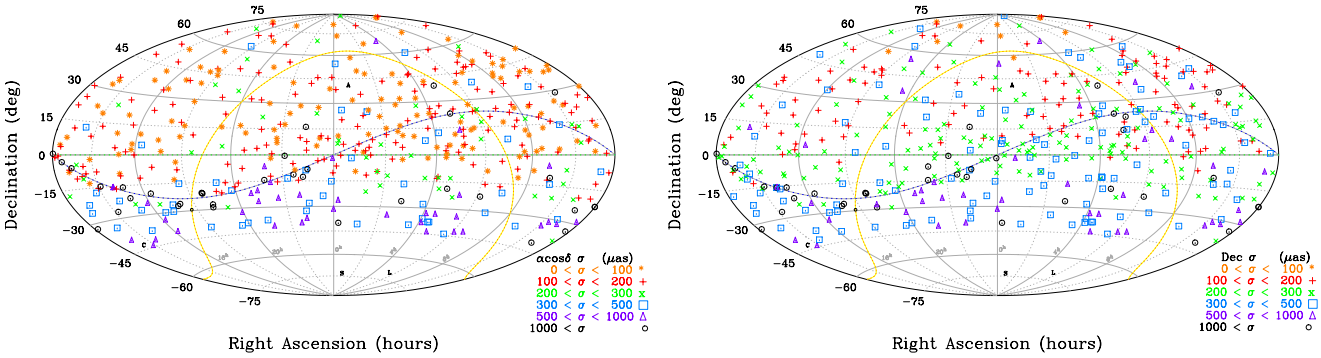

1a. Right Ascen. formal uncertainty: $\sigma_{\alpha\cos\delta}$.

1b. Declination formal uncertainty: σ_δ.

Figure 1. Distribution of 482 X/Ka sources plotted using a Hammer-Aitoff projection to show their locations on the sky. $\alpha = 0$ is at the center. The ecliptic plane is shown by the dashed blue-gray line and the Galactic plane is indicated by the yellow-red dashed line. The sources are color and symbol coded according to their 1-σ formal $\alpha\cos\delta$ and δ uncertainties with the value ranges indicated in the legend. Note the drop in precision below $\delta = -20^\circ$ beyond which the CA-Spain baseline coverage can no longer reach.

An estimate of the accuracy of our source positions was made by comparing 460 X/Ka sources in common with the international standard ICRF2 at S/X-band (2.3/8.4 GHz). The weighted RMS agreement was approximately 180 μas in $\alpha\cos(\delta)$ and 270 μas in δ.

6. Discussion of Errors

Having presented the distribution of position uncertainties in Figs. 1a and 1b above, we now take a closer look at the sources of these uncertainties. We will discuss random errors from white noise, instrumental errors from thermal expansion of the cables and other parts of the signal chain, instrumental errors from changes in antenna pointing direction, tropospheric refraction errors, and ionospheric errors. Table 1 gives rough estimates of the size of each these errors.

Table 1. XKa VLBI Errors

Error	Size
Thermal (random)	12–50 psec
Instrumental: diurnal	∼200 psec
Instrumental: geometric	∼10 psec
Troposphere	∼30–50 psec
Ionosphere	1–30 psec

The systematic weakening of geometry as one moves southward is of special significance and will be treated separately Sec. 7 which follows this section.

6.1. Random Errors

While we are fortunate to have access to the DSN's large 34-meter antennas, cryogenically cooled amplifiers with wide bandwidth (31.7–32.3 GHz), and high rate data recorders (0.5 Gbps, soon to be 2.0 Gbps), system sensitivity remains a major source of error in our measurements. There are several factors which contribute to this situation. First, the source flux densities are typically 0.1 to 1.0 Jy (Jy $= 10^{-26}\ Watt/m^2/Hz$) which even after signal focussing by a large antenna and amplification by low noise electronics still results in a very small signal. Second, antenna performance at Ka-band (9 mm wavelength) is quite challenging. The surface must be smooth to a fraction of a wavelength and the antenna must be pointed to a fraction of a beamwidth ($1.22\ \lambda/D = 1.22\ x$ 9.4 mm / 34m $=$ 19 mdeg). Given the desire to achieve pointing accuracy to 0.1 λ/D, pointing of our large 34-m dishes is quite a challenge. Rochblatt *et al* discuss our pointing system in detail [30]. The atmosphere also contributes to our random errors. The atmosphere absorbs part of the Ka-band signal and emissions from the 22 GHz water line and the 60 GHz O_2 line both increase the system temperature by 7–20K $/\sin(elevation)$. At our lowest elevations of 6° this amounts to 70–200K which dominates the system temperature. Fortunately, advances in digital recording technology make it affordable to compensate to a large degree by recording more bits so that the noise can be averaged down [39]. Specifically, our X/Ka program started with 56 Mbps at Ka-band and has now advanced to 288 Mbps. We hope to be at 2048 Mbps within the next few years. At this 2 Gbps data rate, the white noise contribution will no longer dominate for our average-strength source.

6.2. Systematic Errors

In addition to random errors, there are several sources of non-random errors due to systematic effects: instrumentation, troposphere and ionosphere.

6.2.1. Instrumentation

The data set discussed in this paper was acquired using the Mark-4 Data Acquisition Terminal. These systems use analog 7-pole Butterworth filters and baseband converters designed in the early 1980s and last refurbished in 1997. They are old and difficult to maintain and as a result introduce significant instrumental error. To correct this issue, we are moving to Digital Back Ends (DBE) which use digital phase linear Finite Impulse Response (FIR) filters and digital downconversion for the baseband conversion. García-Miró *et al* [10] discuss our implementation of this concept which is being done in partial collaboration with other efforts in the VLBI community e.g. [31] and [37].

While we expect the DBE to make great improvements in the back end, we still expect to suffer from phase instabilities in the signal transfer from the front end to the back end over cables that can be up to 10 km long—although, in fairness, most of the cable length is buried and it is the exposed non-temperature controlled sections of cable that are most problematic. Our long range plan for correcting this issue is to move the signal's analog-to-digital conversion to the front end to be as near to the first stage RF-to-IF downconverter as practical. This scheme would time tag the data before transmission to the back end and thus remove any cable instabilities.

While we await this technology, we are implementing a phase calibration system to measure and calibrate the cable delays. The system was designed by Hamell *et al* [12]. The calibrators are now built and the process of field deployment has begun. We expect that these calibrators will remove large 100–200 psec diurnal signatures from our data due to temperature changes in our cables.

6.2.2. Tropospheric Fluctuations

Perhaps the most difficult error to deal with is tropospheric turbulence. The components of the atmosphere exclusive of the water vapor ('dry') are reasonably well behaved in the sense of being in near-hydrostatic equilibrium and thus can be calibrated by scaling the surface pressure to a signal delay at zenith and then mapped to the elevation of the observations with so-called mapping functions.

On the other hand, atmospheric water vapor which resides in the lower few km of the atmosphere is not evenly distributed and cannot be predicted based on surface measurements. The water vapor suffers from a turbulent distribution which makes it very difficult to model. Our approach is two-fold. First, we have increased the sophistication of our noise model used for weighting the data. Second, we have developed advanced calibration techniques for measuring the line-of-sight water vapor.

Weighting model: While many analysts in the VLBI world choose to model tropospheric noise with an uncorrelated white noise (Gaussian) distribution, we have found it advantageous to introduce a correlated noise model based on a Kolmogorov distribution. Our implementation was developed by Treuhaft & Lanyi [36] who assume that a static Kolmogorov distribution is carried over the antenna site by a steady wind of $\sim$10 m/s. The result is a model which has both spatial and temporal correlations. Applying this refined weighting model improves the current X/Ka reference frame by about 7%. This improvement appears to be modest until one considers the alternative of obtaining that 7% by acquiring 14% more data which represents about one year's effort at our historical pace.

Water Vapor Radiometers (WVR): While improved data weighting helps to get optimal solutions from noisy data, the ultimate solution is to calibrate out the water vapor fluctuations. Our approach is to use Waver Vapor Radiometers (WVR) which monitor the 22 GHz water emission along the line of sight. Our design is described in two reports by Tanner *et al* [34] [35]. This design improved upon previous WVRs by tightening the radiometer beam from 7° to about 1° in order to better match the tropospheric volumes measured by the WVR and the VLBI antenna. The other key was improving the gain stability. Tests on the 8000 km California-Spain baseline demonstrate that the WVR can calibrate water vapor fluctuations down to the 1 mm (3 psec) level of delay [1].

Once we reduce the random noise with higher data rates and reduce instrumental errors with improved back end filtering and phase calibration, we expect that WVR calibrations will be the key to reducing our overall errors.

6.2.3. Ionosphere

Dual frequency calibration of charged particle effects was used for the great majority of the observations. However, for five sessions the 2nd frequency (X-band, lower) was not available thus resulting in some residual error on the order of 30 psec which is expected to have some dependence on day vs. night due to solar stimulation of the Earth's ionosphere as well as a long term modulation from the 11-year solar cycle.

7. Geometry: Improving the VLBI Network in the South

The DSN is an excellent instrument for astrometric measurements due to its high sensitivity (large apertures, low system temperatures, high data rates) and long baselines ($>$ 8000 km). However, the DSN's single southern site limits the southernmost observed declinations ($\delta > -45^\circ$). In order to better understand the impact of southern geometry, we simulated the effect of adding a second southern station [3]. Data from 50 real X/Ka sessions (Fig. 1c) were augmented by simulated data for 1000 group delays each with SNR $= 50$ on a $\sim$9000 km baseline: Australia to South America (Fig. 1d). A baseline from Australia to a South African site such as HARTRAO would produce a similar geometric improvement.

The resulting solution (Fig. 1d) extended the δ coverage to the south polar cap region: -45° to -90°. Precision in the south cap region was $\sim$200 μas (1 nrad) and in the mid-south precision was 200–1000 μas, all with just a few days observing. We conclude that adding a second southern station would greatly aid our X/Ka frame's coverage and accuracy. In fact, the resulting four station network should compete well in astrometric accuracy with the historical S/X network.

Accordingly, efforts are now under way to improve the DSN southern coverage. We have initiated a project to survey candidate sources at Ka-band in the South Hemisphere [13]. In addition to the candidate survey, we have initiated a collaboration with the European Space Agency to join their 35-m X/Ka-band antenna in Malargue, Argentina to NASA's Deep Space Network [16] to form a much improved network geometry (Fig. 2).

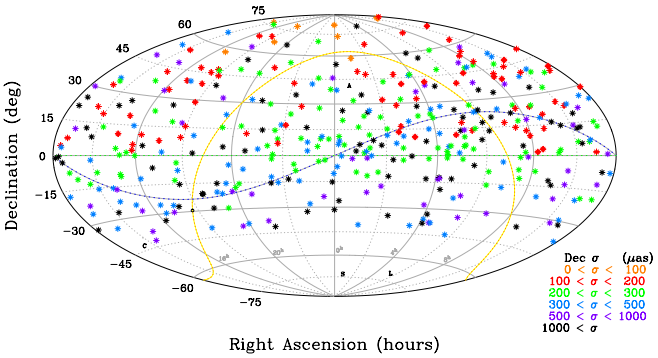

Fig. 1c: Real data from first 50 sessions. Note (1) the complete lack of coverage over the south polar cap: $-45^\circ < \delta < -90^\circ$. (2) the lack of any sources with δ precision $\leq$ 200 μas in the mid-south: $0^\circ < \delta < -45^\circ$.

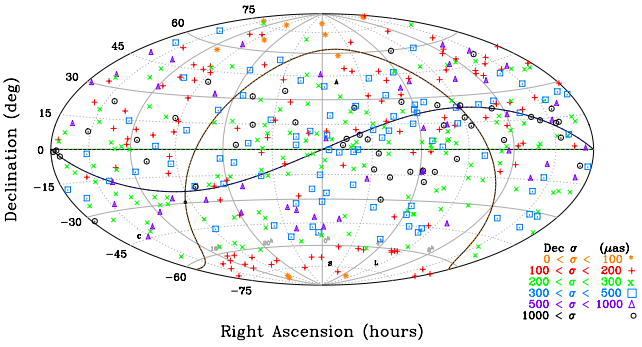

Fig. 1d: Simulated data for 1000 delays added to 50 real sessions completes southern coverage in the south polar cap $-45^\circ < \delta < -90^\circ$. Note that south circumpolar sources ($\delta < -60^\circ$) achieve 200 μas precision within days.

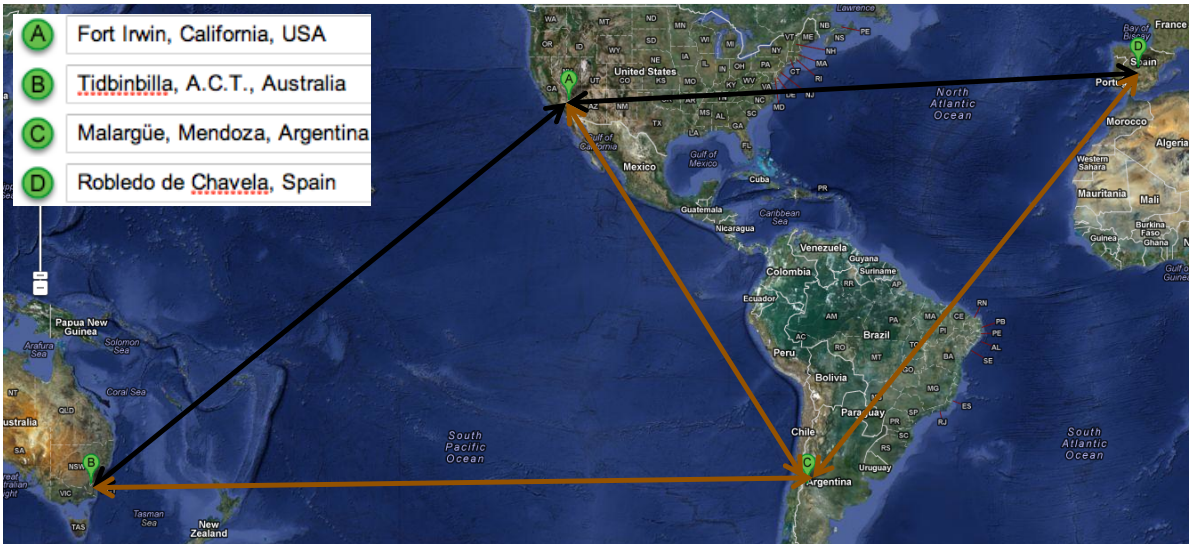

Figure 2. X/Ka Network Geometry: The addition of ESA's Deep Space Antenna (DSA) 03 at Malargue, Argentina adds three new baselines (brown lines: CB, CA, CD) to the already existing pair of NASA Deep Space Network baselines (black lines: AB, AD). The Australia-Argentina baseline (BC) will allow for the first time X/Ka observations of the south polar cap ($\delta < -45^\circ$). *Credit: Google maps.*

8. Tying the X/Ka Radio and Gaia Optical Reference Frames

The future Gaia optical reference frame ([19] and [20]) will also use quasars as defining sources—most of them optically bright. We present here a simulated frame tie between a set of common sources in our X/Ka frame and the Gaia frame. The Gaia mission will survey about a billion objects down to $V = 20$ visual magnitude (500–600 nm), with accuracies ranging from 25 μas at $V = 16$ to ~ 200 μas at $V = 20$. The sample will include about 500,000 quasars of which ~ 2000 are expected to be both optically bright ($V < 18$) and radio loud (30–300+ mJy).

A potential tie between the optical Gaia frame and the radio reference frames requires a deep understanding of the different emitting regions in relativistic jets. For an ensemble of relativistic electrons with an energy power-law distribution which are subjected to synchrotron radiative losses that decrease their lifetimes with increasing energy, the observed flux density distribution becomes more compact but weaker at higher observing frequencies [17]. Moreover, opacity effects, which alter the position of the core, are greatly reduced for higher frequencies. The expected core shift for phase delays from X to Ka is ~ 100 μas and from Ka to optical is ~ 25 μas. However, Porcas [28] argues that, under minimum energy conditions or (near) equi-partition of particle and magnetic energy in the jets [26], the effect in group delay is much smaller than in phase delay. Thus our X/Ka group delay results are expected to have very little core-shift.

Based on the compilation of Veron-Cetty & Veron [38], our X/Ka catalog has 353 sources with optical counterparts bright enough to be detected by Gaia ($V < 20$ mag, Fig. 3, Table 2). Of these, 138 are bright by Gaia standards ($V < 18$).

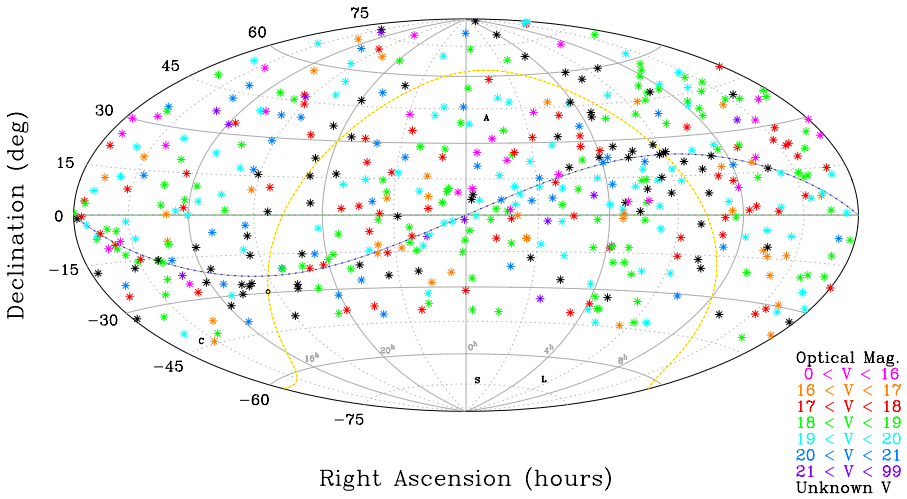

Figure 3. Visual magnitude of optical counterparts for distribution of 482 X/Ka sources. The V magnitude scale is defined in legend. Note the large number of sources lacking optical identifications near the galactic plane (dashed yellow line), especially near its center ($\alpha = 17^h45^m$, $\delta = -29°$) and anti-center.

Table 2. Optical magnitude categories of DSN X/Ka sources

Description	Magnitude range	Number	Percent
Bright	$0 < V < 18$	138	29 %
Detectable	$18 < V < 20$	215	45 %
Undetectable	$20 < V$	53	11 %
Unmeasured	V unknown	76	15 %

Using existing X/Ka-band position uncertainties and simulated Gaia uncertainties [20] (*corrected for ecliptic latitude, but not for V−I color*), we did a covariance study which predicts that the 3-D rotation between the X/Ka frame and the Gaia frame could be estimated with a precision of 10–15

μas per rotation angle (1-σ). The result is dominated by X/Ka uncertainties which have potential for a factor of two or more improvement by the time of the final Gaia catalog in 2021. Thus a frame tie precision of 5–10 μas may be possible.

Table 3. Estimated precision of X/Ka to Gaia frame tie

Angle	Formal Uncertainty
R_x	± 16 μas
R_y	± 13 μas
R_z	± 11 μas

9. Conclusions

Celestial reference frames are useful for spacecraft navigation because they are highly stable and accessible from anywhere in the Solar System. Given the need of modern space missions for nano-radian level angular position measurements, the only viable solution at present for building a sufficiently accurate and stable reference frame is radio interferometric observations of Active Galactic Nuclei. While the current standard for radio frames is based on S/X-band (2.3/8.4 GHz) data, we are moving to X/Ka-band (8.4/32 GHz) for several reasons. First, Ka-band will allow much higher telemetry rates between the spacecraft and the Earth. Second, X/Ka-band allows us to drop S-band which is increasingly plagued by radio frequency interference (RFI). Third, the source morphology is more compact at X/Ka than at S/X-band thereby allowing for a more accurate and stable reference frame to be constructed. While these advantages are significant enough to warrant our course of action, there are several disadvantages which must be overcome before we succeed. The sources tend to be weaker, antenna pointing more difficult, system temperatures higher and more susceptible to degradation from bad weather, and coherence times shorter. All of these combine to disadvantage the system sensitivity. However, the rapidly decreasing costs of recording higher data rates is allowing us to quickly compensate for sensitivity issues.

At present we have detected 482 sources covering the full northern hemisphere and the southern hemisphere down to $\delta > -45^\circ$. The accuracy based on comparisons to the ICRF2 is about 200 μas in Right Ascension and about 30% worse in declination on average. However, in the south the declination accuracy rapidly degrades to being several times worse.

We are optimistic about the potential of the X/Ka-band reference frame for future improvements. The rapid increase of data rates is solving the sensitivity issue. Our nascent collaboration with ESA's site in Malargue, Argentina has the potential to improve significantly our network geometry resulting in robust, uniform all-sky coverage for the first time at X/Ka-band. Also, the source astrophysics is on our side. In moving from S/X to X/Ka-band, the source morphology becomes more compact and core shift is greatly reduced. These factors allow for a superior ultimate accuracy and stability of the X/Ka frame relative to S/X frames. For all these reasons, we believe that X/Ka-band is the direction to take for radio reference frame development.

Acknowledgement: This research was carried out at the Jet Propulsion Laboratory, California Institute of Technology, under a contract with NASA. Government sponsorship acknowledged.

10. References

[1] Bar-Sever, Y. E., C. S. Jacobs, S. Keihm, G. E. Lanyi, C. J. Naudet, H. W. Rosenberger, T. F. Runge, A. B. Tanner, Y. Vigue-Rodi, 'Atmospheric Media Calibration for the Deep Space Network,' Proc. IEEE, vol. 95, issue 11, pp. 2180–2192, Nov. 2007.
http://ieeexplore.ieee.org/stamp/stamp.jsp?arnumber=04390031
http://adsabs.harvard.edu/abs/2007IEEEP..95.2180B

[2] Bessel, F.W., 'On the parallax of 61 Cygni,' Mon. Not. Royal Astron. Soc., 4, 152–161, 1838.
http://adsabs.harvard.edu/abs/1838MNRAS...4..152B
http://articles.adsabs.harvard.edu/cgi-bin/nph-iarticle_query?1838MNRAS...4..152B&data_type=PDF_HIGH&whole_paper=YES&type=PRINTER&filetype=.pdf

[3] Bourda, G., et al., 'Future Radio Reference Frames & Gaia Link,' Proc. ELSA Conf., France, 2010.
http://wwwhip.obspm.fr/gaia2010/IMG/pdf/Poster_Bourda.pdf
http://adsabs.harvard.edu/abs/2011EAS....45..377B

[4] Bradley, J., 'Giving an Account of a New Discovered Motion of the Fix'd Stars,' Phil. Trans. Royal Soc., 35, 637–661, 1727.
http://adsabs.harvard.edu/abs/1727RSPT...35..637B

[5] Bradley, J., 'Concerning an Apparent Motion Observed in Some of the Fixed Stars,' Phil. Trans. Royal Soc., 45, 1–43, 1748.
http://adsabs.harvard.edu/abs/1748RSPT...45....1B

[6] Charlot, P., et al., 'CRF at 24 & 43 GHz II. Imaging,' AJ, 139, 5, 1713, 2010.
http://iopscience.iop.org/1538-3881/139/5/1713/

[7] Fricke, W., et al, 'Fifth fundamental catalogue (FK5). Part 1: The basic fundamental stars,' Verffentlichungen Astron., Rechen-Institut Heidelberg, Verlag G. Braun, Karlsruhe, 2, 1–106, 1988.
http://adsabs.harvard.edu/abs/1988VeARI..32....1F

[8] Folkner, W., P. Kuchynka, 'Linking the planetary ephemerides to the ICRF,' Joint Discussion 7, IAU Gen. Assembly XXVIII, Beijing, China, 2012.
http://www.referencesystems.info/uploads/3/0/3/0/3030024/folkner.pdf

[9] Gaia, 2012.
http://www.rssd.esa.int/index.php?project=GAIA&page=Science_Performance
The above web page in turn references:
de Bruijne, J., M. Perryman, L. Lindegren, C. Jordi, E. Hog, D. Katz, M. Cropper, 'Gaia astrometric, photometric, and radial-velocity performance assessment methodologies to be used by the industrial system-level teams,' Technical Note Gaia-JdB-022, 09 June 2005.

http://www.rssd.esa.int/SYS/docs/ll_transfers/project=PUBDB&id=448635.pdf

[10] García-Miró, C., et al, 'VLBI Data Acquisition Terminal modernization at the Deep Space Network,' Proc. of IVS GM, Madrid Spain, 2012.
http://www.oan.es/gm2012/show_oneabstract.php?id=36
http://www.oan.es/gm2012/pdf/oral_id_36.pdf

[11] Halley, E., 'Considerations on the Change of the Latitudes of Some of the Principal Fixt Stars,' Phil. Trans. Royal Soc., 30, 736–738, 1717.
http://adsabs.harvard.edu/abs/1717RSPT...30..736H

[12] Hamell, R., B. Tucker, and M. Calhoun, 'Phase Calibration Generator,' NASA JPL IPN Progress Report, 42-154, pp. 1–14, 15 Aug. 2003.
http://tmo.jpl.nasa.gov/progress_report/42-154/154H.pdf

[13] Horiuchi, S., et al., '32 GHz CRF Survey Dec $< -45°$,' Proc. of IVS GM, Madrid Spain, 2012.
http://www.oan.es/gm2012/show_contribution.php?id=85
http://www.oan.es/gm2012/pdf/oral_id_85.pdf

[14] Jacobs, C.S., M.B. Heflin, G.E. Lanyi, O.J. Sovers, and J.A. Steppe, 'Rotational Alignment Altered by Source Position Correlations,' Proc. of IVS 2010 General Meeting, Hobart, Tasmania Australia, 8–11 Feb 2010, eds. D. Behrend and K. D. Baver, NASA/CP-2010-215864, Dec. 2010.
http://ivscc.gsfc.nasa.gov/publications/gm2010/jacobs2.pdf

[15] Jacobs, C.S., et al., 'The Potential for a Ka-band Worldwide VLBI Network,' Proc. Journées Conf., Vienna, Austria, 2011.
http://adsabs.harvard.edu/abs/2011kbcn.confE...1J
http://info.tuwien.ac.at/hg/meetings/journees11/Pres/S2/S2_07_Jacobs.pdf

[16] Jacobs, C.S., et al., 'The Celestial Reference Frame at X/Ka-band: Status & Prospects for Improving the South,' The 11th EVN Symposium, Bordeaux, France, 9–12 October, 2012.
http://evn2012.obs.u-bordeaux1.fr/documents/presentations/121_Jacobs_EVN2012_Oral.pdf

[17] Konigl, A., 'Relativistic Jets as X-ray and gamma-ray Sources,' ApJ, 243, 700, 1981.
http://articles.adsabs.harvard.edu/cgi-bin/nph-iarticle_query?1981ApJ...243..700K

[18] Lanyi, et al., 'CRF at 24 & 43 GHz I. Astrometry,' AJ, 139, 5, 1695, 2010.
http://iopscience.iop.org/1538-3881/139/5/1695

[19] Lindegren, et al., 'The Gaia Mission: Science, Organization, and Present Status,' IAU 248, Wenjin et al. (eds.), 217, 2008.

http://journals.cambridge.org/action/displayAbstract?fromPage=online&aid=1930112&fulltextType=RA&fileId=S1743921308019133

[20] Lindegren, et al., 'The astrometric core solution for the Gaia mission,' A&A, 538, Feb. 2012. http://dx.doi.org/10.1051/0004-6361/201117905 http://www.aanda.org/index.php?option=com_article&access=doi&doi=10.1051/0004-6361/201117905&Itemid=129

[21] Lowe, S.T., *Theory of Post-BlockII VLBI Observable Extraction*, JPL Publication 92-7, Jet Propulsion Laboratory, Pasadena, CA, 15 July 1992. http://ntrs.nasa.gov/archive/nasa/casi.ntrs.nasa.gov/19940009399_1994009399.pdf

[22] Lowe, S.T., *SOFTC: A Software VLBI Correlator*, JPL section 335 internal document, Jet Propulsion Laboratory, Pasadena, CA, 29 April 2005.] http://adsabs.harvard.edu/abs/2006ntb..rept...43L

[23] Ma, C., et al., *IERS Technical Note No. 35: The Second Realization of the ICRF by VLBI*, IERS Tech Note 35, Frankfurt, Germany, 2009. http://www.iers.org/nn_11216/IERS/EN/Publications/TechnicalNotes/tn35.html

[24] Mathews, P. M., T. A. Herring, and B. A. Buffet, 'Modeling of Nutation and Precession: New nutation series for Nonrigid Earth and Insights into the Earth's Interior,' JGR, vol. 107, no. B4, 10.1029/2001JB000390, Apr. 2002. http://www.agu.org/journals/jb/jb0204/2001JB000390/

[25] O'Connor, T., 'Introduction to the BlockII Correlator hardware,' JPL internal publication, 08 July 1987.

[26] Pacholczyk, A.G., *Radio Astrophysics*, p. 171, W.H. Freeman, 1970. http://adsabs.harvard.edu/abs/1970ranp.book.....P

[27] Perryman, M.A.C., et al, The HIPPARCOS Catalogue,' A&A, 323, L49–L52, 1997. http://adsabs.harvard.edu/abs/1997A&A...323L..49P

[28] Porcas, R.W., 'Radio Astrometry with Chromatic AGN Core Positions,' A&A letter, v. 505, no. 1, pp. L1–L4, Oct. 2009. http://www.aanda.org/articles/aa/full_html/2009/37/aa12846-09/aa12846-09.html

[29] Ratcliff, J. T. and R. S. Gross, 'Combinations of Earth Orientation Measurements: SPACE2009, COMB2009, and POLE2009,' JPL Publication 10-22, Jet Propulsion Laboratory, Pasadena, CA, Dec. 2010. http://hdl.handle.net/2014/41512 http://trs-new.jpl.nasa.gov/dspace/bitstream/2014/41512/1/JPLPUB10-04.pdf

[30] Rochblatt, D., P. Richter, P. Withington, M. Vazquez, and J. Calvo, 'New Antenna Calibration Techniques in the Deep Space Network,' NASA JPL IPN Progress Report, 42-169, pp. 1–34, 15 May 2007.
http://tmo.jpl.nasa.gov/progress_report/42-169/169A.pdf

[31] Ruszczyk, C., et al, 'VLBI 2010 using the RDBE and Mark5C,' Proc. of IVS GM, Madrid Spain, 2012.
http://www.oan.es/gm2012/pdf/oral_id_126.pdf

[32] Shambayati, S., D. Morabito, J. S. Border, F. Davarian, D. Lee, R. Mendoza, M. Britcliffe, and S. Weinreb, 'Mars Reconnaissance Orbiter Ka-band (32 GHz) Demonstration: Cruise Phase Operations,' in *Proc. AIAA 9th Int. Conf. on Space Operations*, Rome, Italy, 19 Jun 2006.
http://trs-new.jpl.nasa.gov/dspace/bitstream/2014/39654/1/06-0902.pdf

[33] Sovers, O.J., J.L. Fanselow, and C.S. Jacobs, 'Astrometry and Geodesy with Radio Interferometry: Experiments, Models, Results', Rev. Mod. Phys., vol. 70, no. 4, pp. 1393–1454, Oct. 1998.
http://link.aps.org/doi/10.1103/RevModPhys.70.1393

[34] Tanner, A.B., 'Development of a High Stability Water Vapor Radiometer,' Radio Science, 33, 2, pp. 449–462, March-April 1998.
http://www.agu.org/journals/rs/v033/i002/97RS02749/97RS02749.pdf

[35] Tanner, A.B., A. L. Riley, 'Design and Performance of a High-Stability Water Vapor Radiometer,' Radio Science, 38, 8050, 2003.
http://adsabs.harvard.edu/abs/2003RaSc...38.8050T

[36] Treuhaft, R. N. and G. E. Lanyi, 'The Effect of the Dynamic Wet Troposphere on Radio Interferometric Measurements,' Radio Science, 22, pp. 251–65, 1987.
http://www.agu.org/journals/rs/v022/i002/RS022i002p00251/

[37] Tuccari, G., 'DBBC3 - A full digital implementation of the VLBI2010 backend,' Proc. of IVS GM, Madrid Spain, 2012.
http://www.oan.es/gm2012/show_oneabstract.php?id=130
http://www.oan.es/gm2012/pdf/oral_id_130.pdf

[38] Veron-Cetty & Veron, 'Catalogue of quasars and active nuclei: 13^{th} edition,' A&A, 51, Feb. 2010.
http://dx.doi.org/10.1051/0004-6361/201014188

[39] Whitney, A., et al, 'Mark-6 Next Gen VLBI Data System,' Proc. of IVS GM, Madrid, Spain, 2012.
http://www.oan.es/gm2012/show_oneabstract.php?id=22
http://www.oan.es/gm2012/pdf/oral_id_22.pdf